Microstructural investigations of Ni and Ni2Al3 coatings exposed in biomass power plants

Wu, D. L.; Dahl, K. V. ; Christiansen, T. L.; Montgomery, M.; Hald, J.

Published in:
Materials at High Temperatures

Link to article, DOI:
10.1080/09603409.2017.1389382

Publication date:
2018

Document Version
Peer reviewed version

Microstructural investigations of Ni and Ni_2Al_3 coatings exposed in biomass power plants

D. L. Wu*, K. V. Dahl, T. L. Christiansen, M. Montgomery and J. Hald

Department of Mechanical Engineering, Technical University of Denmark, Produktionstorvet building 425, DK-2800 Kgs. Lyngby, Denmark

*Corresponding author, email: duoliw@mek.dtu.dk

The present work investigates the corrosion resistance of Ni and Ni_2Al_3 coated austenitic stainless steel (TP347H) tubes, which were exposed in a biomass-fired boiler with an outlet steam temperature of 540ºC for 6757 h. The Ni_2Al_3 coating was produced by electroplating Ni followed by low temperature pack cementation. After exposure, microstructural investigations were performed by light optical and electron microscopy (SEM-EDS). Electroplated Ni coatings were not protective in straw firing power plants and exhibited similar corrosion morphology as uncoated tubes. For Ni_2Al_3 coatings, the nickel aluminide layer was no longer adherent to the tube and was only found within the deposit. However, Ni_2Al_3 coatings had provided some protection compared to uncoated and Ni coated tubes. The formation of nickel chloride binds aggressive chlorine and slows down the active oxidation mechanism. In local areas, sulphidation corrosion attack of Ni was detected.

Keywords: high temperature corrosion; biomass firing; Ni_2Al_3 coatings; plant testing; KCl

Introduction

The fireside environment in biomass boilers is more corrosive than in coal-fired boilers since hot-section components within biomass boilers are surrounded by corrosive species such as reactive alkali salts (NaCl and KCl), HCl and SO_2 [1]. To avoid excessive corrosion rates, the outlet steam temperature in biomass plants has to be limited to 540 ºC [2]. However, if a corrosion resistant coating could be applied, this would allow an increase in steam temperature resulting in comparable efficiencies to coal firing.

In recent years, there have been promising achievements for corrosion resistant coatings in simulated biomass combustion environments. Hussain et al. [3] evaluated the performance of a thermal sprayed FeCrAl coating in simulated coal-biomass co-fired combustion gases at 700, 750 and 800 ºC for 1000 h. They reported that the FeCrAl coating provided good protection to the steel substrate at 700 ºC but suffered from aggressive corrosion damage at 750 and 800 ºC. It must be noted that coal-biomass co-firing results in conversion of KCl to potassium aluminium silicates and/or potassium sulphate in the combustion zone, and therefore the corrosiveness of the environment is reduced [4]. Vokal et al. [5] investigated the corrosion performance of Fe_2Al_5, (Fe,Ni)Al and Ni_2Al_3 aluminide coatings in air with KCl/K_2SO_4 deposits at 650 ºC for 300 h. The results showed that the Fe_2Al_5 coating was largely unaffected, while the other two coatings were significantly corroded. They attributed the intergranular corrosion of the two coatings to chromium enrichment along the grain boundary. Kiamehr et al. [6] investigated the performance of two pack aluminised iron-based coatings ($Fe_{1-x}Al$ and Fe_2Al_5) and one nickel based coating (Ni_2Al_3) at 600 ºC for 168 h in static lab air with a KCl deposit. It was reported that Ni_2Al_3 showed no sign of attack, however, $Fe_{1-x}Al$ showed local attack and Fe_2Al_5 suffered heavily from selective aluminium removal. After testing for 168 hours at 560˚C in an atmosphere simulating flue gas from a straw-firing

plant (6 vol. % O_2, 12 vol. % CO_2, 400 ppmv HCl, 60 ppmv SO_2, balance N_2 on dry basis; the dry gas being led through a heated humidifier resulting in a final H_2O content of 13.4 vol. %) localised aluminium depletion was found for an Ni_2Al_3 diffusion coating [7].

The present investigation evaluates the corrosion performance of Ni, Ni_2Al_3/Ni coated and uncoated reference tube sections welded into the superheater of a biomass combustion boiler and exposed for 6757 h. Testing in the actual boiler environment allows evaluation of parameters that are difficult to simulate simultaneously in the laboratory such as thermal cycling, thermal stability, corrosive environment, flue gas dynamics and temperature, heat fluxes and deposition formation. The evaluation of plant exposed coatings gives invaluable input as to the actual degradation mechanisms, and the information can be used to modify the coatings to avoid specific failure mechanisms as well as to design future laboratory experiments to replicate the relevant failure mechanisms.

Experimental procedure

Coating preparation

The austenitic stainless steel TP347H (Fe-18Cr-12Ni-2Mn-0.07C-<1.2(Nb+Ta)-<0.75Si wt. %) was used as substrate material. Tube sections (Outer diameter (OD) 32 mm, inner diameter (ID) 19 mm, length of 200 mm) were cut from a TP347H tube and were coated with a) electrolytical Ni b) Ni_2Al_3 coating. The Ni coating was electroplated using a Watts nickel-plating solution. The plating was performed at 45 ^oC with a current density of 6 A/dm^2 for 100 minutes. The Ni plated tubes were heat-treated (650 ^oC + 1 h, Ar+H_2) to strengthen the bonding between the steel and the nickel layer. The Ni_2Al_3 coating was prepared by a two-step process where nickel was first electroplated as previously described followed by low temperature pack aluminising. For aluminising, the

Ni coated tube sections were then embedded in pre-mixed pack powders (10 wt. % Al + 8 wt. % $AlCl_3$ + 82 wt. % Al_2O_3), which were put into a cylindrical metal crucible and inserted into a tube furnace with argon flow. The furnace was heated to 650 ºC with a heating rate of 18 ºC/min, and held for 6 h. Afterwards, the samples were cooled inside the furnace by switching off the power while maintaining the argon flow.

After processing, the Ni and Ni_2Al_3 coated tube sections were cleaned with ethanol. To make the tube sections ready for welding, the coatings were removed by machining a 2 cm wide area from both ends of the Ni and Ni_2Al_3 coated tube sections. The coated Ni, Ni_2Al_3 and uncoated reference tubes are shown in Figure 1.

Figure 1. Morphology of (a) Ni coated, (b) Ni_2Al_3 coated and (c) uncoated tubes

Power plant exposure

Tube sections coated with Ni, Ni_2Al_3 and uncoated were welded into one of the leading tubes of the outlet superheater of a Danish straw-fired biomass boiler located at Maribo Sakskøbing with an outlet steam temperature of 540ºC and were exposed for 6757 h before removal for investigations.

Sample preparation and characterization

The exposed tubes after removal from the power plant are shown in Figure 2. Prior to removal of the tubes, the superheater had to be cleaned and this resulted in removal of deposit and some of the surface corrosion products. The Ni_2Al_3 coated tube was covered with a thick layer of corrosion product together with deposit in most areas. Some of the corrosion product and deposit was scraped off the tube and prepared for analysis. Lesser amounts of deposit were present for the Ni coated tube and uncoated tube.

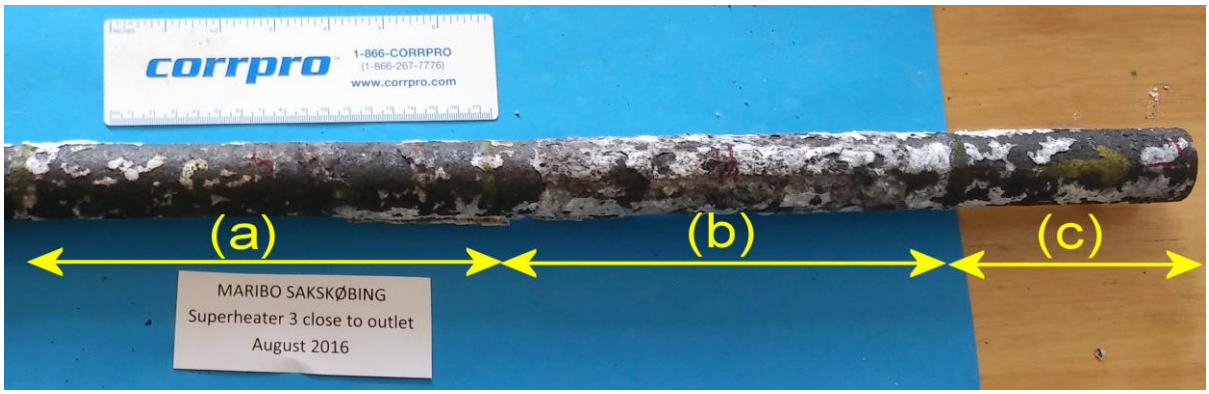

Figure 2. Morphology of (a) Ni coated, (b) Ni_2Al_3 coated and (c) uncoated tubes after boiler exposure

The tube sections were cut into thin rings (5-7mm) from the middle of each tube section in dry condition, and were embedded in epoxy resin. In order to reduce dissolution of water-soluble compounds, grinding and polishing were performed using absolute ethanol as lubricant. Grinding was performed using SiC paper, while polishing was done with diamond slurry until a final step of 1 µm diamond. The cross-sections were examined using a scanning electron microscope (FEI Quanta 200 ESEM FEG) equipped with energy dispersive X-ray Spectroscopy (Oxford Instruments 80 mm^2 X-Max) for chemical analysis. Image acquisition was performed in back-scattered electron (BSE) mode with high vacuum.

Results

Ni and Ni_2Al_3 coatings before exposure

The Ni and Ni_2Al_3 coatings were uniform with smooth interfaces and surfaces (Figure 3). The Ni-Al coating consisted of an outer Ni_2Al_3 layer (thickness variation between 50 and 70 µm) and an inner Ni layer (100 µm) and was adherent to the steel. The Ni_2Al_3 layer was identified by XRD (not shown). A very thin (<5 µm) layer of intermediate phases could be seen at the interface between Ni and Ni_2Al_3. Porosities could be observed at the Ni/steel interface. The Ni coating consisted of a single Ni layer with a thickness of about 125 µm.

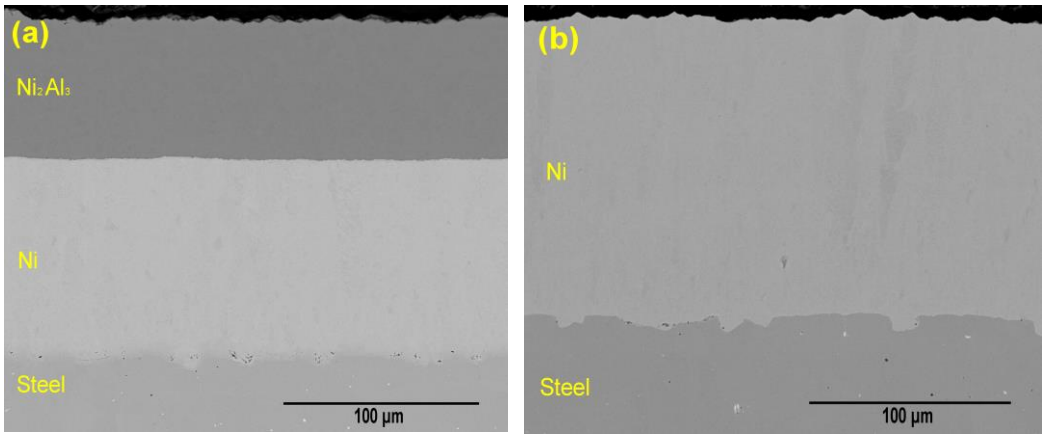

Figure 3. BSE-SEM micrograph of cross-section of (a) Ni_2Al_3 coated and (b) Ni coated tube sections

Ni and Ni_2Al_3 coatings and reference tube after exposure

Metal loss thickness was measured around the circumference of the tubes. The thickness varied greatly as shown in Table 1, and this can depend on the varying initial thickness of the tube (wall thickness 5.6 mm and production tolerances ±10%) but also the positioning of the tube with respect to flue gas direction. It was therefore decided to focus on the morphology of attack to gain increased understanding on the breakdown of the coating. The morphology of uncoated, Ni coated and Ni_2Al_3 coated tubes after exposure are described in the following sections.

Table 1. Residual metal thickness around the circumference of the tubes

	Residual metal thickness (mm)		
	Min	Max	Average
Uncoated tube	4.498	5.250	4.922
Ni coated tube	4.749	5.142	4.976
Ni_2Al_3 coated tube	4.545	5.341	5.057

Microscopy analysis of uncoated tube

Different corrosion morphologies were evident on the exposed uncoated tube. In some areas, an oxide layer was present with limited underlying grain boundary attack (Figure 4), while deep grain boundary attack was observed in other areas (Figure 5). The corrosion product consisted of an outer oxide, an inner selective corrosion area and grain boundary attack. The oxide located in the outermost corrosion product was rich in iron, and the oxide below was rich in chromium. There was selective corrosion attack beneath the oxide, and chromium depletion was detected together with nickel enrichment (EDX results in Figure 4). Enrichment of chlorine was identified close to the corrosion front in the selective corrosion area. The indications of silicon enrichment close to the selective corrosion area were probably due to use of SiC papers in the grinding process.

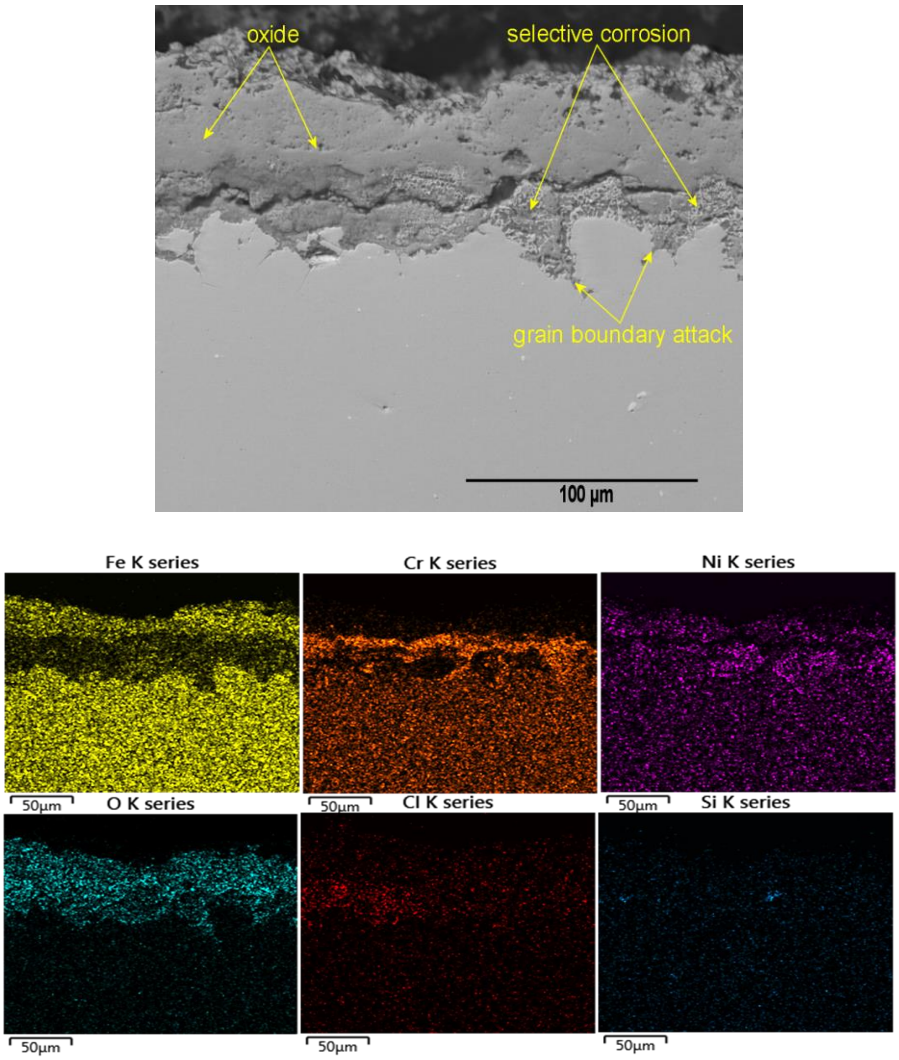

Figure 4. SEM/BSE image of the corrosion morphology and EDX chemical element distribution for the uncoated tube after boiler exposure

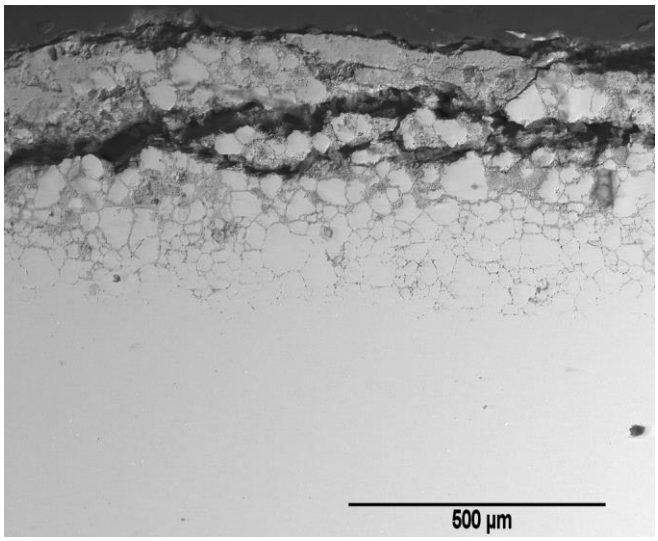

Figure 5. SEM/BSE image of corrosion morphology showing deep grain boundary attack in the uncoated tube after boiler exposure.

Microscopy analysis of Ni coated tube

The morphology of corrosion products and chemical element distribution are given in Figure 6. The pure Ni layer was no longer present on the Ni coated tube after exposure. A voluminous corrosion product was formed at the outermost surface. The corrosion products were rich in iron and nickel in the outer part and rich in chromium in the inner part. Clear enrichment of chlorine was observed close to the underlying metal.

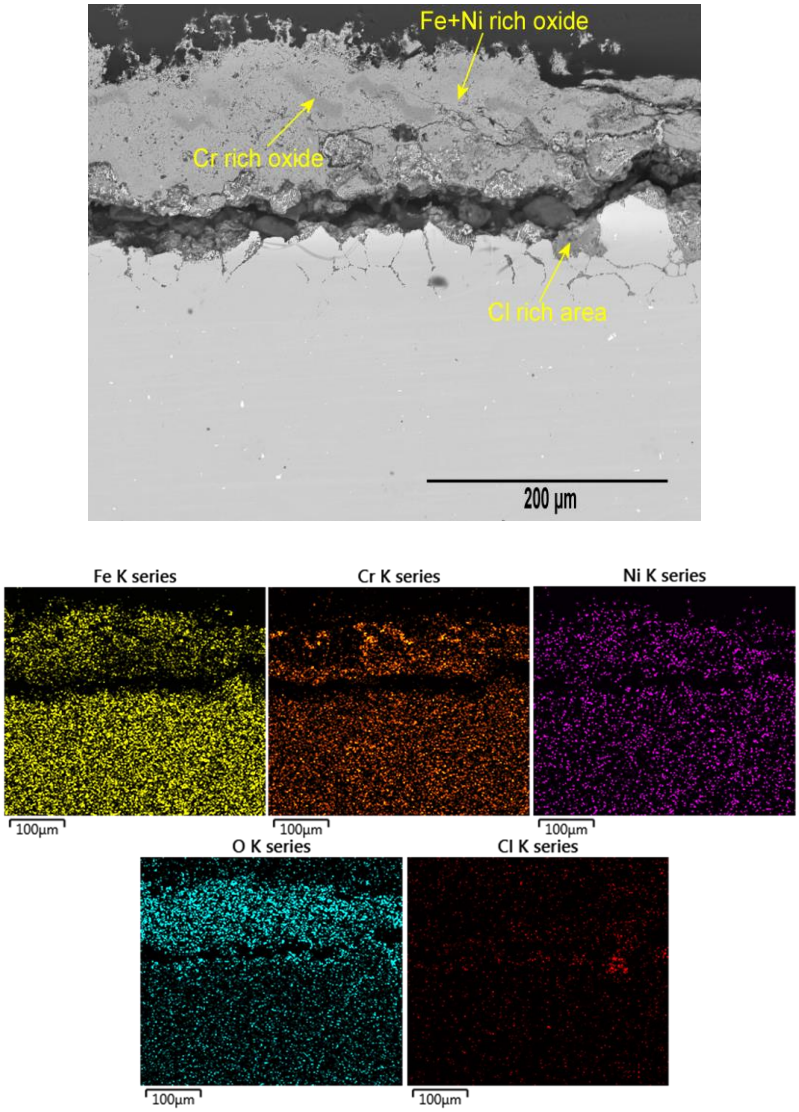

Figure 6. SEM/BSE image of corrosion morphology and EDX chemical element distribution for Ni coated tube after boiler exposure

Localised grain boundary attack could be seen in locations with voluminous outer oxide, while deeper grain boundary attack was apparent in areas with thinner corrosion products (Figure 7), similar to the findings for the uncoated tube. Since the KCl was not revealed on cross-sections, some surface oxide could have spalled during tube removal and handling.

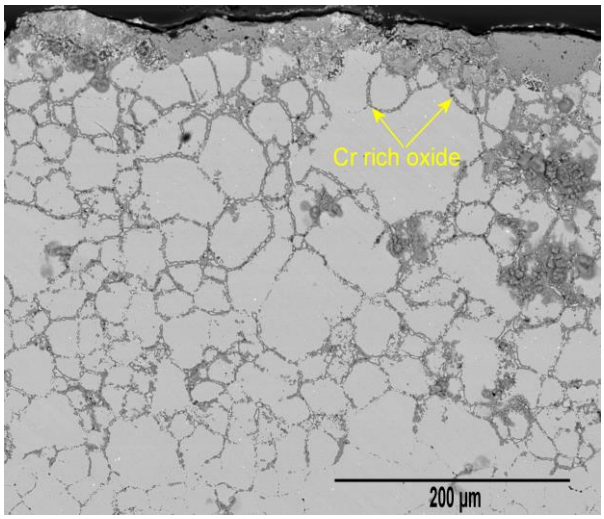

Figure 7. SEM/BSE image of a location with severe grain boundary attack for Ni coated tube after boiler exposure

Microscopy analysis of Ni_2Al_3 coated tube

After boiler exposure, the Ni_2Al_3 coated tube exhibited two distinct corrosion features, a) where there were no remnants of the coating and only the TP347H tube was present and b) where the electroplated Ni layer was still present. Areas where the Ni layer was absent were similar to the attack on the uncoated TP347H tube, see Figures 4-7. Where the electroplated Ni layer was present, it is assumed that the Ni_2Al_3 layer had peeled off as no evidence of aluminium was observed within the corrosion products (Figure 8). Remnants of the Ni_2Al_3 layer could be found in the deposit (described later in this section), further supporting this assumption. Figure 8 reveals an area where the nickel layer is present above the stainless steel tube material (shown in the maps as Cr and Fe rich). At locations above the Ni-layer, SEM/EDX revealed the presence of both

potassium and chlorine within the deposit indicating the presence of potassium chloride, and therefore no spallation of corrosion products during handling.

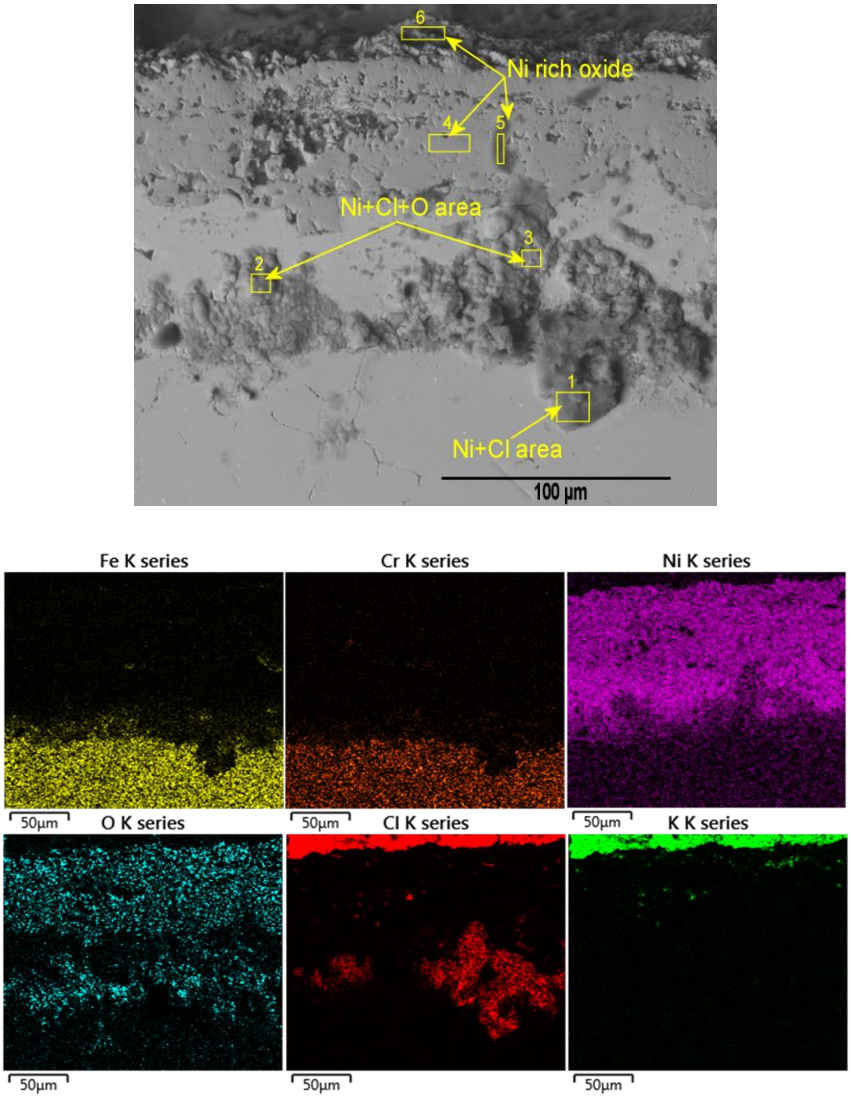

Figure 8. SEM/BSE image of corrosion morphology and element distribution on the Ni_2Al_3 coated tube after boiler exposure at a location where the Ni layer was present. In the SEM image, location of EDX measurements was reported in Table 2.

SEM-EDS analysis shows that the external oxides are rich in nickel only (Table 2). A large area with chlorine enrichment could be identified below the nickel enriched outer oxide. Above the nickel coating-TP347H interface, the chlorine species are associated with nickel (region 2 and 3), however within the TP347H layer, the Cl species are associated with Ni, Fe and Cr (region 1). The morphology of the Cl species seems to indicate that they have emerged from the metallic material after polishing and that they

are sitting on top of the polished section. The EDX analysis could therefore include both the compound sitting on the surface and the underlying polished surface.

Table 2. Elemental composition of selected regions in Figure 8.

	Elemental composition (wt. %)				
region	Cl	Ni	O	Fe	Cr
1	35.1	24.5		35.0	5.4
2	26.7	40.1	24.0	8.9	0.4
3	30.5	47.0	18.7	3.8	
4		84.6	15.4		
5		79.4	20.6		
6		84.8	15.2		

At other locations, where the nickel layer was still present, a large part of the original nickel layer remained with a thickness of about 70 µm (Figure 9a). In some areas, a thick zone of mixed corrosion products could be found above the nickel layer (Figure 9b).

SEM/EDX (Figure 9a and Table 3) show a local area of Cr-rich oxide close to the surface (region 3) and sulphur enrichment in the outer surface (regions 5 and 6) as well as within sulphur rich phases in the nickel layer. The absence of K and Cl on the surface could indicate that the surface corrosion products have been removed during removal and handling of the tubes. Cl enrichment as well as severe grain boundary attack were observed in the underlying TP347H metal. Cl was distributed everywhere where there was grain boundary attack and enriched in localised places (regions 1 and 2).

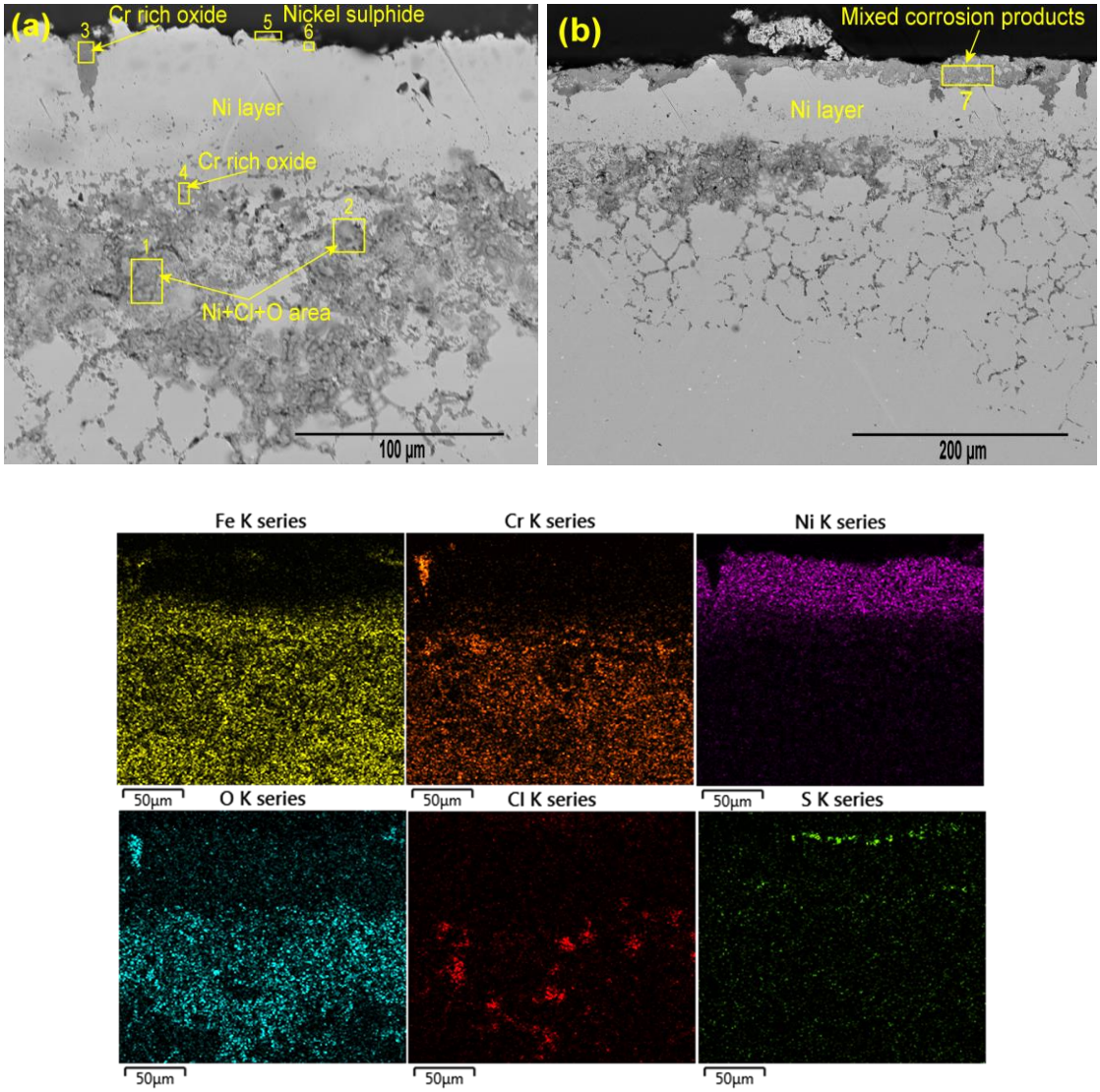

Figure 9. SEM/BSE of corrosion morphology on the Ni_2Al_3 coated tube after boiler exposure for locations with (a) nickel layer and (b) nickel layer with outer corrosion product and EDX chemical element distribution corresponding to (a). Compositions of selected areas in (a) and (b) are shown in Table 3.

Table 3. Elemental composition of selected regions in Figure 9a and 9b.

	elemental composition (wt. %)						
region	Cl	Ni	O	Fe	Cr	Mn	S
1	11.4	13.9	14.6	48.2	10.5	1.4	
2	10.3	16.8	11.0	52.1	9.8		
3			23.7	17.4	58.9		
4			15.8	41.1	43.1		
5		77.9					22.1
6		80.1					19.9
7		49.4	14.1	32.7	3.8		

Microstructure and element distribution in the deposit for Ni_2Al_3 coated tubes

Within the deposit, remnants of the Ni_2Al_3 coating could be found, and their analysis can give further information as to how the attack progressed on the Ni_2Al_3 coated tubes. The corrosion morphology and the distribution of chemical elements in the deposit are shown in Figure 10. The top part of the micrograph was closest to the flue gas environment. The coating element aluminium, which was absent at the tube surface locations, was observed in the deposit of Ni_2Al_3 coated tubes. A multi-layered oxide scale that must have spalled from the tube surface could be found intact in the deposit. The oxide scale had a porous nickel-rich oxide scale at both sides and an aluminium-rich oxide in between. A number of blocky structured potassium chloride particles are dispersed on the top of the multi-layered oxide scale.

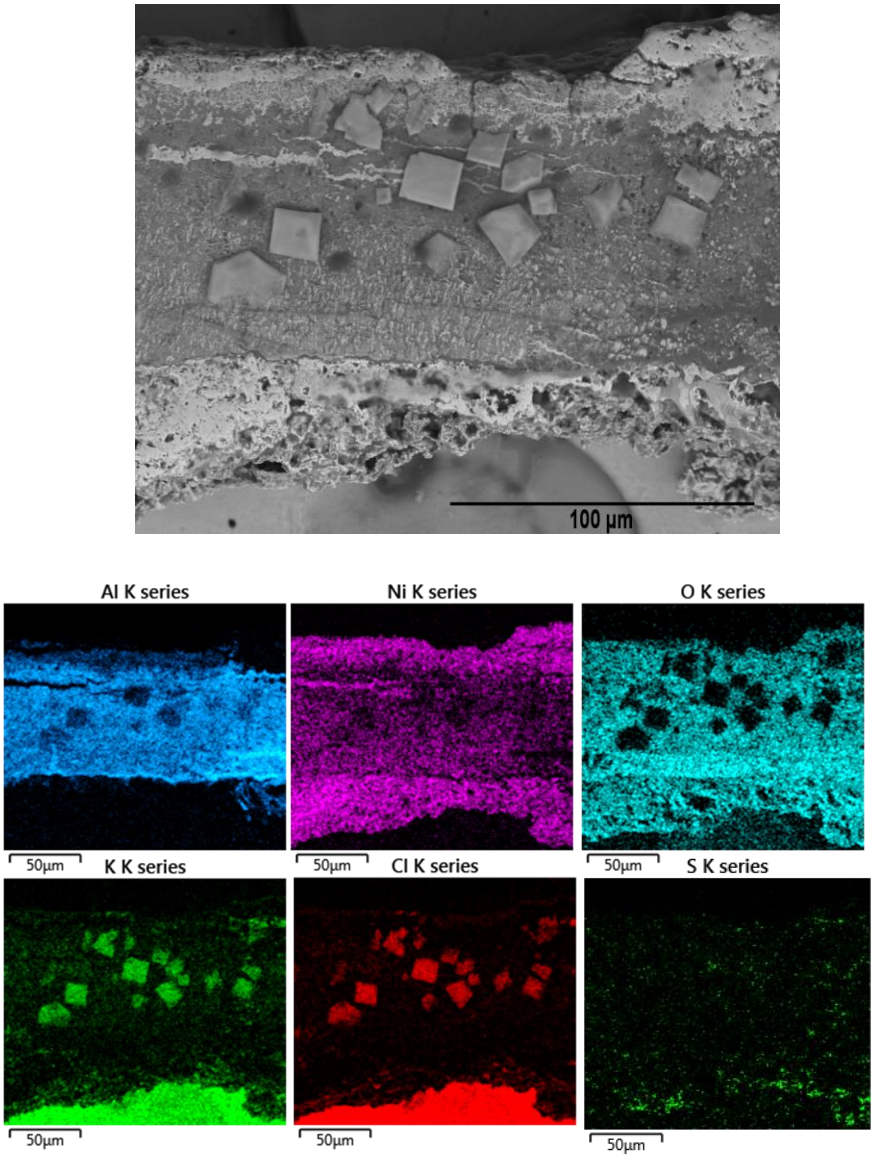

Figure 10. Corrosion morphology and element distribution of the deposit on Ni_2Al_3 coated tube after boiler exposure.

A composition profile measured by EDS shows that the concentration of aluminium is around 30 wt. % in the centre of the spalled scale, which should still be sufficient for the formation of protective aluminium oxide (Figure 11). The two peaks in the aluminium profile lie on each side of a Ni-rich band, which is visible as a white layer within the aluminium-rich oxide.

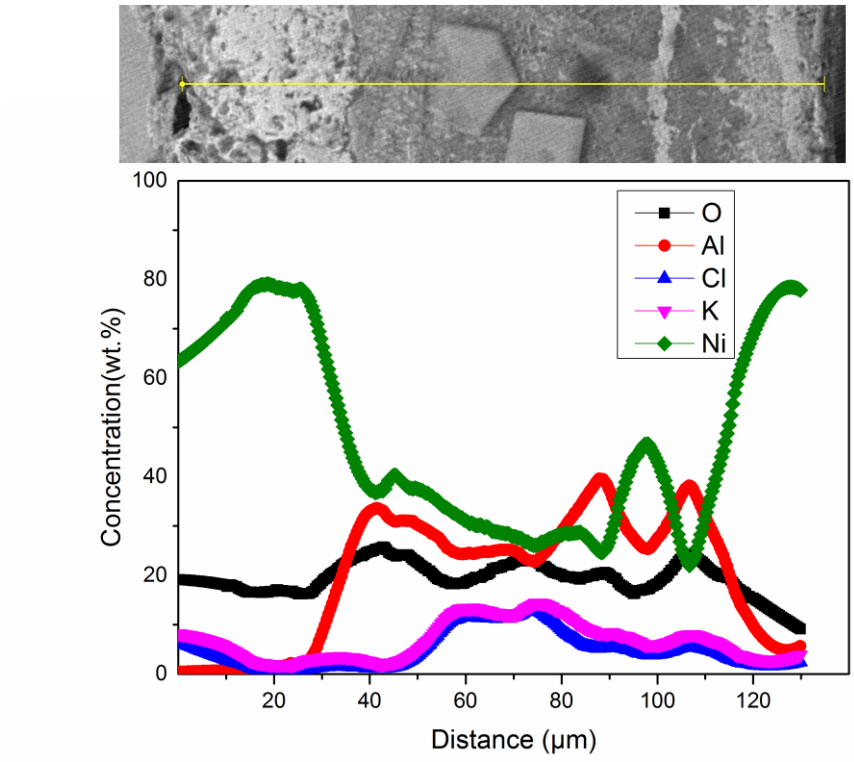

Figure 11. Composition profiles measured by EDS of the deposit on Ni_2Al_3 coated tube after boiler exposure.

Discussion

Uncoated tube

The corrosion morphology on the uncoated TP347H tube was similar to previously published research results from both laboratory and field testing [8–10]. The corrosion product was composed of an outer iron-rich oxide closest to the flue gas environment and chromium-rich oxide below this. A region of selective corrosion was found beneath the oxides with grain boundary attack penetrating into the steel at the corrosion front. In biomass combustion, the corrosion mechanism due to the aggressive alkali chlorides has been extensively investigated [11–15]. The initiation of corrosion is based on breakdown of protective oxide due to reaction of KCl with the oxide [6], and the propagation of corrosion is due to reaction with Cl species [16,17]. However even in environments with

high HCl content, increased corrosion is also observed [16,17] which indicates that a protective oxide is vulnerable when other Cl species are present. The observed corrosion morphologies in this study can be explained by the widely used active oxidation mechanism [17], after the initial breakdown of the protective oxide either by HCl or KCl attack. In the active oxidation mechanism, chlorine species penetrate the oxide layer and form metal chloride within the bulk metal. At high temperatures, the volatile metal chlorides sublime and diffuse outwards to form oxides where the partial pressure of oxygen is higher. The conversion of chromium chloride to oxides occurs at low partial pressures of oxygen, and therefore chromium rich oxides are found at the inner part of the oxide scale, while iron rich oxides are found in the outer part. The cyclic reaction continues with the chlorine released from the formation of oxides.

According to the element distribution in Figure 4, potassium was not present at the corrosion front. Thus, Cl species must have been released, which could be due to reactions between KCl and metal oxides or sulphation of KCl. Cl^- ions could also be generated by reaction of HCl and oxygen [13] or via reaction 1.

$$2KCl + \left(\frac{1}{2}\right) O_2(g) + H_2O(g) + 2e^- = 2KOH(g) + 2Cl^- \qquad (1)$$

The released chlorine can then react with chromium, iron and nickel with preferential reaction with chromium due to its high affinity for chlorine. In this way, areas of selective attack with chromium depletion are formed.

Ni coated tube

The Ni coated tube shows similar corrosion morphology as the uncoated tube. The pure nickel layer is no longer present, indicating that the nickel layer was not protective during the biomass boiler exposure. In fact, the corrosion attack is more severe than on the uncoated tube, however it is not known how much corrosion product has spalled during removal of the tube from the plant. In laboratory investigations by Jonsson et al. [18] the

corrosion rate of pure Ni was not affected by the addition of small amounts of KCl, which probably indicates that the increased complexity of the exposure environment plays a role in the failure of the Ni-plated tubes. Okoro et al. [16] investigated the corrosion performance of Ni-coated Esshete 1250 under more complex conditions mimicking biomass combustion with addition of sulphur. Under these conditions, Ni was attacked and a porous Ni-rich oxide was formed after exposure. Cl species as well as S rich precipitates were identified, which indicated both chlorination and sulphidation attack. It was speculated that mechanical failure of the Ni coating led to easy migration of sulphur to the coating/metal interface. In the present case, such mechanical failure of the layer could easily happen during start/stop procedures. Ansey [19] exposed tubes electroplated with nickel in waste incineration plants and suggested that the nickel layer recrystallised on heating to 560 ºC and therefore gave paths for intergranular attack of Ni. It is suggested that the nickel is also attacked and therefore itself is not a barrier against attack. However, since no remnants of the Ni-layer were present, the exact mode of attack remains unclear, and after removal of the Ni layer the stainless steel tube was attacked. It must however be assumed that thermal cycling was not a main reasons of failure, since the Ni layer was still present in many areas on the Ni_2Al_3 coated specimen.

Ni_2Al_3 coated tube section

The corrosion morphology of the Ni_2Al_3 coated tube is different from the Ni coated tube in many places, which indicates that the Ni_2Al_3 coating did not spall immediately at the start of exposure. However, the nickel aluminide layer was no longer adherent to the tube and was only found within the deposit (Figure 10), while remnants of a nickel layer (up to 70 µm) were present in many locations (Figures 8 and 9) with varying depths of attack of the underlying tube. From previous laboratory isothermal interdiffusion testing at higher temperatures, it was noted that porosities developed at the interface of the Ni-

Al/Ni and expanded with time [7]. For the coatings exposed in real superheater tubes, the formation of porosities would be more serious in combination with thermal cycling, which would probably lead to spallation of the nickel aluminide layer. The spalled coating reveals further interesting findings. The surface of the Ni_2Al_3 spalled coating is nickel rich, which indicates that Al has been depleted. Thus, a single layer of protective alumina has not been formed giving protection, but instead the aluminium has gradually and selectively been consumed during exposure. The Al content within the middle of the spalled coating is still high, which could indicate that had it adhered to the tube, it could have given some protection until the Al was totally consumed. However, it is not known whether the compact aluminium-rich oxide only formed in the middle part of the scale whilst it was still adherent to the tube or only after spallation. If protective Al_2O_3 formed whilst it adhered, this could indicate that it was not the corrosion but instead spallation and possibly interdiffusion that led to coating failure.

Despite the absence of the nickel aluminide layer on the investigated tube cross sections, the Ni_2Al_3 coating still provided protection of the substrate metal at some tube locations, compared to uncoated and the Ni coated tubes. At the location shown in Figure 8 with thick corrosion products, the underlying metal has only been slightly attacked.

Presence of Cl species at the corrosion front

After spallation of the coating, the nickel layer is attacked. Again, it is difficult to know whether the Ni was attacked whilst the Ni_2Al_3 coating was present but had become porous. One of the interesting features, which was only observed for the Ni_2Al_3 coated tubes, is that there is a strong indication of the presence of metal chlorides at the corrosion front (Figure 9). This is observed both within the nickel layer and in the underlying alloy. For the nickel layer, the nickel is first oxidised with the formation of NiO(s). Then Cl species may penetrate the nickel oxide scale into the metal as the oxide is a not a barrier

against Cl diffusion. Underneath the oxide scale, the oxygen potential is low and virtually all of the Cl can be converted to $NiCl_2$. In some places, the $NiCl_2$ (g) will diffuse out and react with oxygen to form NiO(s) [20]. However, nickel chloride is not as easily oxidised and is not as volatile as chromium or iron chloride. Accordingly, nickel chloride is trapped in the metal in locations far from the corrosion surface (region 1 in Table 2), which indicates that nickel and chlorine rich corrosion products are more stable. It is thus suggested that nickel binds the aggressive chlorine and slows down the active oxidation mechanism. In this way, only slight attack occurs in the underlying metal. However, there is attack of the underlying metal, and again metal chlorides are trapped beneath the nickel layer and not oxidised (region 1 in Table 2). This strongly indicates that transport of the Cl species is more likely than transfer of oxygen species and evaporation of metal chlorides. This could indicate that in this case transfer of Cl is mainly via an electrochemical reaction proposed in [13]. Without the coating, the metal chlorides migrate to locations with higher partial pressures of oxygen and are oxidised by the incoming oxygen, but this mechanism is hampered by the Ni/Ni_2Al_3 layers.

Presence of sulphide within Ni layer

The nickel and sulphur rich layer indicates the formation of nickel sulphide (Ni_3S_2) on the outer surface and within the nickel layer (regions 5 and 6 in Table 3). The performance of nickel in sulphur containing atmospheres has been widely investigated [21–25]. In the temperature range between 480°C and 620°C, NiO is thermodynamically preferred over Ni_3S_2, even under oxidising SO_2 atmospheres. However, when the gas atmosphere tends to more reducing conditions, the sulphur attack becomes more prevalent [21]. This leads to the formation of Ni_3S_2 by the reaction in equation 4 [26].

$$7Ni + 2SO_2 = 4NiO + Ni_3S_2 \qquad (2)$$

It is speculated that the formation of Ni_2S_3 is because of the presence of a corrosion product above the sulphide layer, as the partial pressure of oxygen must be low to form nickel sulphide. The corrosion product could have been lost during preparation, which is substantiated by the lack of KCl as was observed in Figure 8. As shown in Figure 9(b), there were also areas with thick corrosion products above the nickel layer. The formation of nickel sulphide (Ni_3S_2) could have detrimental effects on the material properties, possibly leading to crack formation. The cracks can then act as channels for both sulphur and chlorine species to diffuse to the underlying metal [19]. The chlorine can react with chromium, iron and nickel to form metal chlorides. The chromium chloride can then migrate out to an area of higher oxygen partial pressure and convert to chromium oxide.

Conclusions

1. Ni coatings do not provide protection in straw firing biomass plants at 540 ^{o}C. The Ni coated tube shows similar corrosion morphology as the uncoated tube and the pure nickel layer is no longer present after exposure.
2. Some protection is observed for Ni_2Al_3 coatings as Ni_2Al_3 coatings do not spall in the initial exposure. However, the nickel aluminide layer is no longer adherent to the tube and is only found within the deposit. Spallation of the nickel aluminide layer is probably due to the formation of porosities.
3. The presence of a Ni_2Al_3 coating hinders evaporation of metal chlorides from the corrosion front, but does not prevent Cl species to diffuse to the corrosion front. Although KCl may break down the oxide, this highlights that it is Cl that propagates the corrosion reaction and is present at the corrosion front.
4. The formation of trapped nickel chloride hampers the corrosion process by binding the aggressive chlorine.

Acknowledgements

This paper was written under the project EUDP 14-I New Coatings for Biomass Firing. The authors also acknowledge financial support from the FORSKEL project "Biomass Corrosion Management".

References

1. Nielsen HP, Frandsen FJ, Dam-Johansen K, Baxter LL. Implications of chlorine-associated corrosion on the operation of biomass-fired boilers. Prog Energy Combust Sci. 2000;26(3):283–298.
2. Montgomery M, Jensen SA., Borg U, Biede O, Vilhelmsen T. Experiences with high temperature corrosion at straw-firing power plants in Denmark. Mater Corros. 2011;62(7):593–605.
3. Hussain T, Simms NJ, Nicholls JR, Oakey JE. Fireside corrosion degradation of HVOF thermal sprayed FeCrAl coating at 700–800°C. Surf Coatings Technol. 2015;268:165–172.
4. Larsen OH, Montgomery M. Materials problems and solutions in biomass fired plants. Energy Mater. 2006;1(4):227–237.
5. Vokál V, Rohr V, Pomeroy MJ, Schütze M. Corrosion of alloys and their diffusion aluminide coatings by KCI:K_2SO_4 deposits at 650°C in air. Mater Corros. 2008;59(5):374–379.
6. Kiamehr S, Lomholt TN, Dahl KV, Christiansen TL, Somers MAJ. Application of aluminum diffusion coatings to mitigate the KCl-induced high-temperature corrosion. Mater Corros. 2016;(1):82–94.
7. Wu D, Okoro SC, Dahl KV, Montgomery M, Pantleon K, Hald J. Laboratory Investigations of Ni-Al Coatings Exposed to Conditions Simulating Biomass Firing. 9th Int Symp Corros Prot Mater. 2016;1–8.

8. Montgomery M, Karlsson A, Larsen OH. Field test corrosion experiments in Denmark with biomass fuels Part I: Straw-firing. Mater Corros. 2002;53(2):121–131.
9. Kiamehr S, Dahl KV., Montgomery M, Somers MAJ. KCl-induced high temperature corrosion of selected commercial alloys: Part I: chromia-formers. Mater Corros. 2015;66(12):1414–1429.
10. Liu C, Little JA, Henderson PJ, Ljung P. Corrosion of TP347H FG stainless steel in a biomass fired PF utility boiler. J Mater Sci. 2001;36(4):1015–1026.
11. Cha SC, Spiegel M. Fundamental Studies on Alkali Chloride Induced Corrosion during Combustion of Biomass. Mater Sci Forum. 2004;461–464:1055–1062.
12. Cha SC, Spiegel M. Local reactions of KCl particles with iron, nickel and chromium surfaces. Mater Corros. 2006;57(2):159–164.
13. Folkeson N, Johansson L-G, Svensson J-E. Initial Stages of the HCl-Induced High-Temperature Corrosion of Alloy 310. J Electrochem Soc. 2007;154(9):C515-C521.
14. Jonsson T, Folkeson N, Svensson JE, Johansson LG, Halvarsson M. An ESEM in situ investigation of initial stages of the KCl induced high temperature corrosion of a Fe-2.25Cr-1Mo steel at 400^{o}C. Corros Sci. 2011;53(6):2233–2246.
15. Folkeson N, Jonsson T, Halvarsson M, Johansson LG, Svensson JE. The influence of small amounts of KCl(s) on the high temperature corrosion of a Fe-2.25Cr-1Mo steel at 400 and 500^{o}C. Mater Corros. 2011;62(7):606–615.
16. Okoro SC. High Temperature Corrosion on Biodust Firing. Technical University of Denmark; 2016.
17. Grabke HJ, Reese E, Spiegel M. The effects of chlorides, hydrogen chloride, and sulfur dioxide in the oxidation of steels below deposits. Corros Sci.

1995;37(7):1023–1043.

18. Jonsson T, Slomian A, Lomholt TN, Kiamehr S, Dahl KV. Microstructural investigations of pure nickel exposed to KCl induced high temperature corrosion. Mater High Temp. 2015;32(1–2):44–49.

19. Ansey JW. Dickschichtvernickeln als korrosionsschutz fur bauteile in kesselanlagen [Thick layer nickel coating as corrosion protection for components in steam generators]. VGB PowerTech. 2003; 83(12): 106–110.

20. Lee YY, McNallan MJ. Ignition of nickel in environments containing oxygen and chlorine. Metall Trans A. 1991;18(6):1099–1107.

21. Bloch HP, Soares C. Application of hot gas turboexpanders. In: Turboexpanders and Process Applications, Elsevier. 2001. p. 238–242.

22. Seiersten M, Kofstad P. The high temperature corrosion of nickel in SO_2 at 500-800^oC. Corros Sci. 1982;22(5):487–506.

23. M. F. Stroosnijder and W. J. Quadakkers. A corrosion study of Ni and Ni-Cr alloys in $SO_2/H_2O/H_2$ atmospheres using gas analysis. 1989;29(9):1059–1072.

24. Quadakkers WJ, Khanna AS, Schuster et al. Investigation of the corrosion mechanisms of nickel and nickel-based alloys in SO_2-containing environments using an evolved gas analysis technique. Mater Sci Eng A. 1989;120-121(1–2 pt 1):117–122.

25. Kofstad P, Akesson G. High-Temperature Corrosion of Nickel in SO_2. 1978;12(6):503–526.

26. Gesmundo F, de Asmundis C, Nanni P. The corrosion of nickel in 1 atm of pure SO_2 at 600-1000^oC and the mechanism of formation of the two-layered scales. Oxid Met. 1983;20(5–6):217–240.